RSC Sustainability

ROYAL SOCIETY OF CHEMISTRY

PAPER

View Article Online
View Journal | View Issue

Cite this: *RSC Sustainability*, 2024, **2**, 3090

Towards green visible range active photocatalytic Au/TiO_2 nanocomposites through rutin-based synthesis and their application in the degradation of ciprofloxacin†

Inês Catarina Gomes Espada, [ab] Noelia González-Ballesteros,[ac] Carlos J. Tavares,[a] Senentxu Lanceros-Méndez*[ade] and Pedro M. Martins *[bf]

Photocatalysis is a low-cost solution to efficiently remove resilient emergent pollutants from wastewater with complex chemical structures, such as pharmaceuticals. Titanium dioxide (TiO_2) is the most studied photocatalyst and is usually functionalised with gold (Au) nanoparticles to prevent electron–hole pair recombination and extend visible radiation absorption. However, conventional synthesis techniques use toxic chemicals and present high energy consumption. The focus of this work is to present and optimize a green synthesis method using the flavonoid rutin – a natural compound found in various plants – as the reducing agent at room temperature to decrease the environmental impact and optimise the chemical, physical, and photocatalytic properties of Au/TiO_2 nanoparticles with concentrations of Au of 0.025, 0.1, and 1 wt%. Through ciprofloxacin (CIP) degradation under UV and simulated solar radiation, enhanced photocatalytic efficiency is observed due to adding Au nanoparticles, proving that rutin is a suitable reducing agent for green nanoparticle synthesis.

Received 18th April 2024
Accepted 10th September 2024

DOI: 10.1039/d4su00186a

rsc.li/rscsus

Sustainability spotlight

This work highlights the sustainable advancement of photocatalytic materials through the green synthesis to functionalize TiO_2 nanoparticles with Au using rutin, aligning with the UN's Sustainable Development Goals, particularly Goal 6 (Clean Water and Sanitation) and Goal 12 (Responsible Consumption and Production). By employing a natural flavonoid for nanoparticle synthesis, this approach minimises environmental impact, reduces energy consumption, and eliminates toxic waste, contributing to more sustainable water treatment methods. The spotlight on the enhanced photocatalytic efficiency under both UV and visible radiation demonstrates the potential for broader application in degrading persistent water pollutants, such as ciprofloxacin, promoting the availability of clean water and the sustainable management of contaminated water matrixes.

Introduction

Water is one of the fundamental necessities for the survival of all beings. However, in 2020, just 74% of the world's population had access to safe water facilities, *i.e.*, contamination-free and available when necessary.[1] Emergent pollutants are non-regulated toxic chemicals found in low concentrations, which are very resilient to conventional wastewater treatments, thus being one of the principal sources of persistent contamination.[2] One example of an organic pollutant found commonly in wastewater is Ciprofloxacin (CIP), an antibiotic used to treat severe bacterial infections, such as pneumonia, conjunctivitis and sexually transmitted infections.[3] Due to its complex chemical structure and high stability, it cannot be efficiently removed in conventional wastewater treatment plants (WWTPs). Consequently, it can damage aquatic ecosystems and, due to bioaccumulation, can be consumed by humans.[4,5] Therefore, developing new, more robust water remediation methods has been extensively studied, and some of the most suitable methods rely on advanced oxidation processes.[6]

Advanced oxidation processes (AOPs) produce oxidising species, such as hydroxyl free radicals ($OH^{\bullet}$), that enable pollutant oxidation and consequent degradation.[7] Among these processes, photocatalysis represents a promising low-cost solution for water remediation due to its photochemical

[a]*Physics Centre of Minho and Porto Universities (CF-UM-UP), LaPMET – Laboratory of Physics for Materials and Emergent Technologies, University of Minho, 4710-057 Braga, Portugal. E-mail: lanceros@fisica.uminho.pt*

[b]*Institute for Research and Innovation on Bio-Sustainability (IB-S), University of Minho, 4710-057 Braga, Portugal. E-mail: pamartins@bio.uminho.pt*

[c]*Universidade de Vigo, Departamento de Química Inorgánica, 36310 Vigo, Spain*

[d]*BCMaterials, Basque Center for Materials, Applications and Nanostructures, UPV/EHU Science Park, 48940 Leioa, Spain*

[e]*IKERBASQUE, Basque Foundation for Science, 48009 Bilbao, Spain*

[f]*Centre of Molecular and Environmental Biology (CBMA), University of Minho, 4710-057 Braga, Portugal*

† Electronic supplementary information (ESI) available. See DOI: https://doi.org/10.1039/d4su00186a

stability and high efficiency.[8] Typically, photocatalysis involves irradiating a semiconductor material – the photocatalyst – by ultraviolet (UV) or visible radiation. If the incident energy is equal to or higher than the photocatalyst's band gap, its absorption will lead to the transition of an electron in an electro-filled valence band (VB) to the conduction band (CB), creating a positive hole (h^+) in the valence band.[9,10] The electron–hole pairs react with H_2O and O_2 to produce highly reactive oxygen species that initiate reactions to degrade pollutants into CO_2, H_2O and other harmless compounds.[11]

TiO_2 is the most used and researched photocatalyst due to its abundance and low cost. Furthermore, it possesses unique optical properties, chemical and thermal stability, chemical resistance to decomposition, low toxicity, and good oxidising properties.[12–14] However, it has some disadvantages, such as aggregation due to its small size when used in the form of nanoparticles, the high recombination of electron–hole pairs and low photocatalytic activity under visible radiation because of its band of 3.2 eV.[15] This problem can be solved through the functionalisation with noble metals, such as gold (Au), silver (Ag), copper (Cu), and cobalt (Co). If added to the TiO_2 nanoparticle surface, these metals can receive electrons, preventing the recombination of electron–hole pairs and absorbing visible radiation due to a surface plasmon resonance (SPR) phenomenon.[16]

Although various techniques have been developed to synthesise Au/TiO_2 nanoparticles, toxic chemicals and high energy consumption hamper their implementation on a larger scale.[17] Studies have recently been conducted on green synthesis to reduce pollution by implementing sustainable processes and industries. These new environmentally friendly methods allow the production of nanomaterials with optimised chemical and physical properties while also reducing or even eliminating toxic waste and reducing energy consumption by exchanging the toxic chemicals used as reducing and stabilising agents with natural extracts, such as microorganisms[18] and plants.[19]

Plant-mediated synthesis of nanoparticles is farther stable than those assisted by microbes.[20] This, along with their simplicity, efficiency, and low cost, makes them the most studied natural extract used as reducing and stabilising agents in the green synthesis of nanoparticles, mainly metallic oxides.[10] It must be noted that the 'extracts' properties can suffer daily alterations due to changes in the plant's environment. Therefore, using biomolecules found naturally in plants has gained some interest recently since they can be processed in controlled conditions, guaranteeing the same properties every time.[21] Rutin is a flavonoid glycoside found in citrus fruits and various plants, such as buckwheat, Japanese pagoda tree, and eucalyptus.[22] It possesses good antioxidant, anti-inflammatory, cardioprotective, anticancer, and cholesterol-lowering properties.[23] Dessai, S. *et al.*[24] could synthesise TiO_2 nanoparticles through a rutin-mediated co-precipitation method by adding a rutin solution to titanium tetraisopropoxide (TTIP). They evaluated the nanoparticles' antibacterial, antidiabetic, and antioxidant properties. To the best of our knowledge, there are no recorded works of rutin-based green synthesis of Au/TiO_2 nanoparticles for applications in water remediation through photocatalysis.

In this work, Au/TiO_2 nanoparticles are synthesised with the flavonoid rutin, and their physical and chemical properties are compared to those of pristine TiO_2. The photocatalytic efficiency is tested by degrading CIP under UV and simulated solar radiation to determine the sustainability of the developed approach.

Experimental

Materials

Evonik provided P25 titanium dioxide (TiO_2) nanoparticles. A gold(III) chloride ($HAuCl_4$) solution and rutin hydrate (≥94%) were purchased from Sigma-Aldrich, and AppliChem supplied sodium hydroxide (NaOH) pellets. Milli-Q ultrapure water (resistivity 18.2 MΩ cm) was used in all experiments. Ciprofloxacin (CIP, ≥98% HPLC) ($C_{17}H_{18}FN_3O_3$) with maximum light absorption at a wavelength of 277 nm was supplied by Thermo Fisher Scientific.

Green synthesis of Au/TiO_2 nanoparticles

The Au/TiO_2 synthesis is conducted using a green deposition–precipitation method, which is schematised in Fig. 1. Firstly, 200 mg of TiO_2 P25 nanoparticles are dispersed in 40 mL of ultrapure water in an ultrasonic bath for 30 minutes. 100, 1000

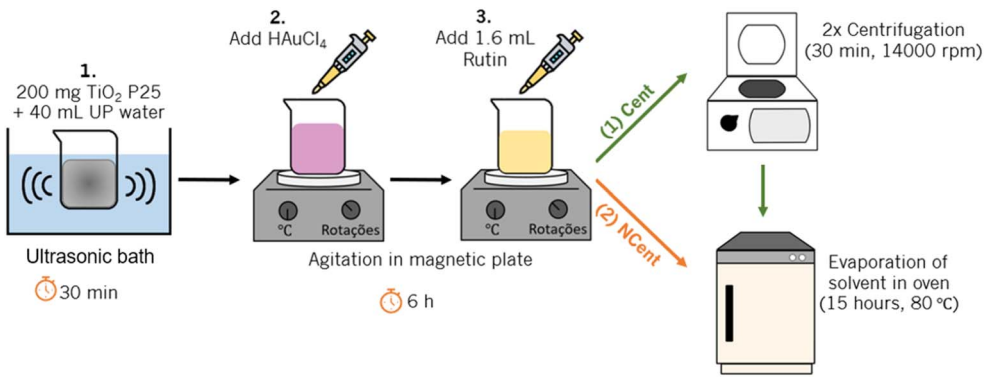

Fig. 1 Schematic representation of the Au/TiO_2 synthesis process.

and 4000 μL of an aqueous solution of $HAuCl_4$ (0.05 wt%) is added to obtain the specific Au concentrations of 0.025, 0.1, and 1 wt%. Afterwards, 1.6 mL of a solution of rutin (0.05 wt%), previously produced by dispersing 12.5 mg of rutin hydrate powder in 25 mL of NaOH (0.1 M), is added. This leads to an Au/rutin ratio of 0.0625, 0.625 and 2.5 for the samples with Au concentrations of 0.025, 0.1, and 1 wt%, respectively. The resultant solution is mixed in a magnetic plate for 6 hours until the colour changes from yellow to purple.

After mixing, half of each sample, marked in the following as "Cent", is centrifuged for 30 minutes (14 000 rpm and at 8 °C). The supernatant is discarded, and 40 mL of fresh ultrapure water is added. The nanoparticles are dispersed with ultrasounds for 2 minutes, and the solution is centrifuged. This process is repeated with 20 mL of ultrapure water. Afterwards, another 20 mL of ultrapure water is added to disperse the nanoparticles, and the solution is dried overnight at 80 °C. The resulting powder is placed in a mortar and grounded. The other half of each sample, marked as "NCent" (non-centrifuged) in the following, is directly placed in the convection oven at 80 °C overnight to dry the supernatant, and the resulting powder are also grounded in a mortar. This allows for the evaluation of the influence of rutin on the nanoparticle properties and photocatalytic efficiency.

Characterisation of the Au/TiO_2 nanoparticles

The morphology of Au/TiO_2 nanoparticles is evaluated by transmission electron microscopy (TEM) using a FEI Tecnai T20. The crystalline structure of the nanoparticles is analysed through X-ray diffraction (XRD) with a Philips diffractometer PW 1710 with radiation Cu Kα (40 kV and 30 mA), corresponding to a wavelength of 1.54 Å. The Scherrer equation[25] is used to derive the average crystallite size:

$$D = (\kappa\lambda)/(\beta \cos\theta), \quad (1)$$

where D is the crystallite size, κ is a dimensionless shape factor with a value of 0.9 due to the spherical shape of the nanoparticles, $\lambda = 1.54$ Å is the wavelength of the X-rays, β is the full width at half maximum (FWHM) of the diffraction peak in the XRD pattern, and θ is the angle at which the maximum peak is observed.

A Zetasizer Nanoseries nano-zs from Malvern Instruments Limited is used to obtain the hydrodynamic sizes and polydispersity index (PDI) of the Au/TiO_2 nanoparticles at pH 3. Zeta potential measurements were also performed at pH 3, 5, 7, 9, and 11. A PerkinElmer Spectrum Two Fourier-transform infrared spectroscopy (FTIR) spectrometer with universal Attenuated Total Reflection (ATR) was used to identify the chemical constitution of the Au/TiO_2. Sixteen scans are carried out per sample, with a wavenumber range from 4000 to 500 cm^{-1}, and the spectra are obtained with the software PerkinElmer Spectrum IR. Finally, the absorbance spectra of the Au/TiO_2 nanoparticles are measured through reflectance spectroscopy with a UV-2501 PC UV-vis Recording Spectrophotometer. Barium sulphate ($BaSO_4$) is used as a reference, and the measurements are carried out in a wavelength range from 240 to 800 nm. The Tauc expression[26] was used to calculate the band gaps of the nanoparticles:

$$(h\nu\alpha)^{1/n} = A(h\nu - E_g), \quad (2)$$

where h is Planck's constant, ν is the vibration frequency, α is the absorption coefficient, A is the proportional constant, and E_g is the band gap energy. Since, in this study, the indirect allowed sample transition is used, $n = 2$.

Photocatalytic degradation of ciprofloxacin

The nanoparticles' photocatalytic activity is tested by degrading a CIP solution (5 mg L^{-1}) under UV and simulated solar radiation. A control sample is withdrawn from this solution. Firstly, 50 mg of nanoparticles are added and stirred in 50 mL of the CIP solution in the dark for 30 minutes to ensure the adsorption–desorption equilibrium.

The UV degradation tests are then carried out in a photoreactor with eight UV Philips lamps of 8 W, with an emission peak at 365 nm (radiation spectra on ESI Fig. 1†). The solutions are irradiated for 60 minutes under continuous agitation. Samples are withdrawn at times 0, 2, 5, 10, 15, 20, 30, 40, 50, and 60 minutes, and the absorption spectra are recorded using a spectrophotometer in the wavelength range between 230 and 400 nm.

For the simulated solar radiation degradation, a xenon lamp of 300 W m^{-2} from Oriel Instruments (radiation spectra on ESI Fig. 2†) with an excitation peak at 550 nm is used to simulate solar radiation. The solutions in agitation are placed 20 cm from the lamp for 3 hours. Samples are withdrawn at times 0, 2, 5, 10, 15, 20, 30, 40, 50, 60, 90, 120, 150, and 180 minutes and the absorption spectra are also measured for the same wavelength range. Both cases follow the Langmuir–Hinshelwood (L–H) pseudo-first-order kinetics model,[27] which simplified equation can describe:

$$C/C_0 = e^{-kt}, \quad (3)$$

where C_0 is the initial CIP concentration, C is the concentration at a time t, and k is the pseudo-first-order constant.

Results and discussion

Characterisation of the Au/TiO_2 nanoparticles

Au/TiO_2 nanoparticles are synthesised with rutin with different Au concentrations (0.025, 0.1, and 1 wt%). Fig. 2 shows the influence of the different Au concentrations on the colour of the nanocomposites synthesised using rutin.

It is observed that the nanocomposites with larger concentrations of Au show a more distinct purple colour. Furthermore, the non-centrifuged nanocomposites show a yellow hue related to the presence of rutin, which is removed by the centrifugation process.

Fig. 3 shows TEM micrographs of the morphology of pristine TiO_2 and synthesised Au/TiO_2 nanoparticles.

The spherical shape of TiO_2 nanoparticles is confirmed for both the pristine and synthesised samples. The presence of the

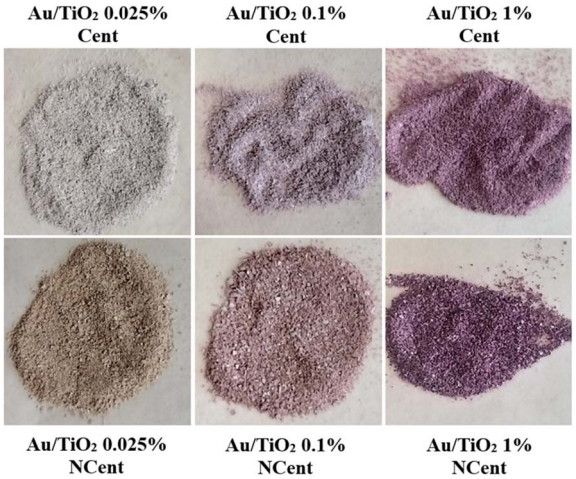

Fig. 2 Influence of different Au concentrations and presence of rutin on the synthesised nanoparticles' colour.

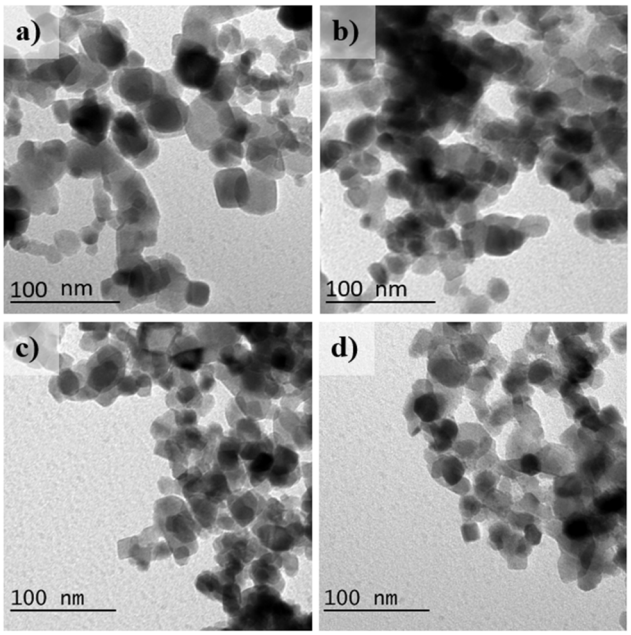

Fig. 3 TEM images of (a) pristine TiO_2 nanoparticles and synthesised (b) Au/TiO_2 0.025% Cent, (c) Au/TiO_2 0.1% Cent, (d) Au/TiO_2 1% Cent nanocomposites.

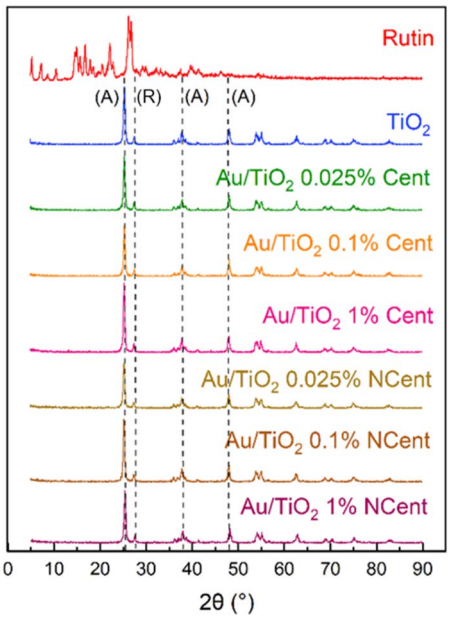

Fig. 4 XRD reflexes of rutin, pristine TiO_2 and synthesised Au/TiO_2 nanoparticles, both centrifuged (Cent) and non-centrifuged (NCent), showing the peaks corresponding to the anatase (A) and rutile (R) crystalline phases.

Au nanoparticles is not observed, as their size is below image resolution.

The pristine TiO_2 nanoparticles have an average size of 21.2 ± 0.5 nm. The nanoparticles with Au concentrations of 0.025, 0.1, and 1 wt% show average sizes of 21.9 ± 0.6 nm, 20.4 ± 0.4 nm, and 20.0 ± 0.5 nm, respectively.

XRD is performed to determine the crystalline structure of rutin, pristine TiO_2 and synthesised nanoparticles (Fig. 4). The typical reflexes from the anatase (25.3°, 37.8°, 48.0°) and rutile (27.5°) phases of TiO_2 are observed in both pristine nanoparticles and nanocomposites, independently of the centrifugation process.[28] No reflexes of Au or rutin are detected since the low concentrations are below the detection limit of the equipment.

The Scherrer equation (eqn (1)) is applied to determine the average crystalline size of the TiO_2 particles in the different samples. The FWHM and the diffraction angle are determined using the Power Cell software. For every sample, $\beta = 0.203°$ and $\theta = 25.31°$. Consequently, the calculated diameter of the crystal is $D = 6.9$ nm for every sample. This further proves that Au or rutin's presence does not change the crystallinity of TiO_2.

The hydrodynamic size distribution histograms (Fig. 5) and the average sizes of pristine TiO_2 nanoparticles and synthesised Au/TiO_2 nanocomposites are determined by DLS at pH 3. The results show an average hydrodynamic size of 283 ± 1 nm for pristine TiO_2. This value is decreased for every functionalised sample, ranging from 144 ± 2 nm to 173 ± 2 nm. The obtained PDI for the synthesised nanocomposites is ~0.15, which indicates a monodisperse sample. For the pristine TiO_2 nanoparticles, the PDI is 0.35, implying a worse size distribution or a polydisperse sample.[29] The presence of Au over the TiO_2 nanoparticle's surface reduces the hydrodynamic size compared to pristine TiO_2.

Table 1 shows the average sizes for every sample obtained through each technique, explaining further the differences in the dimension data obtained by TEM, XRD, and DLS measurements.

Compared to the nanoparticle size measurements by TEM (~20 nm for all analysed samples), the hydrodynamic sizes determined by DLS are significantly larger. This is explained by the fact that the samples used for the TEM measurements are dry. Conversely, the samples in the DLS analysis were dispersed in an aqueous medium, which promotes the formation of

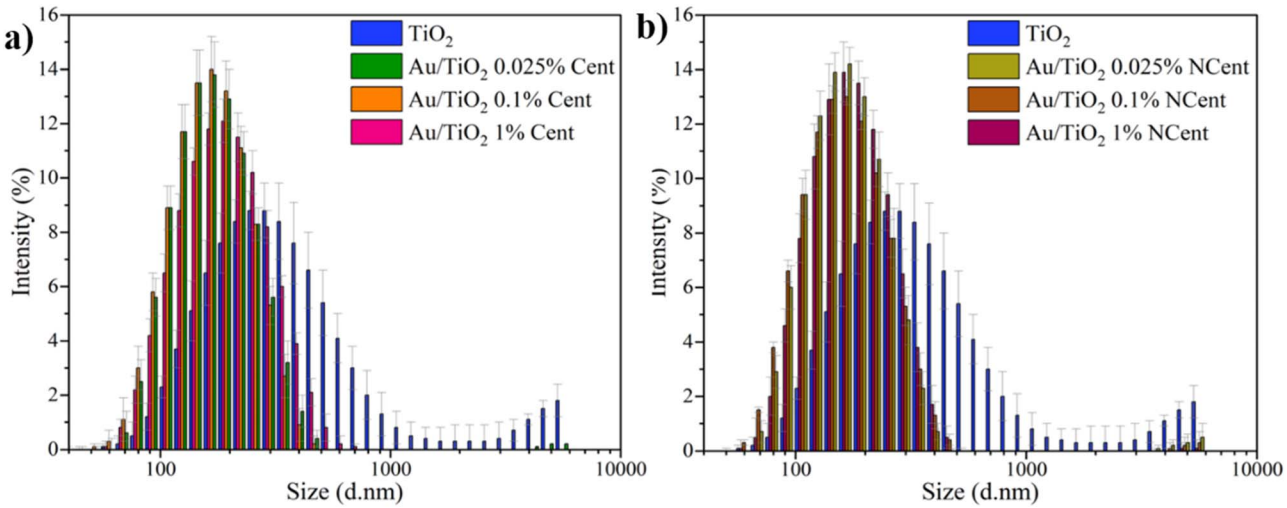

Fig. 5 Hydrodynamic size distribution of pristine TiO_2 and Au/TiO_2 nanoparticles, both (a) centrifuged and (b) non-centrifuged.

Table 1 Summary of the nanoparticle sizes determined by TEM, XRD, and DLS[a]

		Sizes (nm)		
	Sample	TEM	XRD (Scherrer equation)	DLS
	TiO_2	21.2 ± 0.5	6.9	283 ± 1
Cent	Au/TiO_2 0.025%	21.9 ± 0.6		158 ± 1
	Au/TiO_2 0.1%	20.4 ± 0.4		151 ± 2
	Au/TiO_2 1%	20.0 ± 0.9		173 ± 2
NCent	Au/TiO_2 0.025%	ND		153 ± 3
	Au/TiO_2 0.1%			150 ± 1
	Au/TiO_2 1%			162 ± 2

[a] (ND – not determined).

agglomerates that influence the diffusion processes and lead to a larger overall volume producing higher scattering intensities.[30,31] Furthermore, since the hydrodynamic sizes of the nanocomposites from DLS are lower than that of pristine TiO_2, it can be inferred that the functionalisation with Au nanoparticles promotes a higher repulsion between particles in dispersion, leading to lower trends towards agglomeration.[16,32]

The sizes obtained through the Scherrer equation[33] in the XRD measurements show the lowest value (6.9 nm) as it only accounts for the average crystallite size, not the entire nanoparticle size.[34]

The periphery surface charge of the nanoparticles is studied through measurements of the zeta potential for pH 3, 5, 7, 9, and 11 (Fig. 6). Every sample presents positive zeta potential values for acidic pH and negative values for basic pH. The maximum values ($\approx|40|$ mV) are obtained for pH 3 and 11, which is consistent with the literature.[33] The results for the centrifuged and non-centrifuged samples generally present similar behaviour at different pHs. The isoelectric point, in which the particles carry no electrical surface charge, is between pH 5 and 7. For pH 3, approximately the pH of the ciprofloxacin solution used in the photocatalytic tests, the synthesised nanocomposites absolute zeta potential values ($\approx|40|$ mV) are larger than for TiO_2 ($|38.7|$ mV). Notably, larger zeta potential values indicate a higher peripheric surface charge, promoting repulsions between nanoparticles that ensure enhanced stability and prevent aggregation.[16,32] This confirms the DLS results, which show that higher repulsions between nanoparticles avoid the formation of agglomerates and lead to smaller hydrodynamic sizes.

Fig. 7 shows ATR-FTIR results for the produced nanoparticles. In the rutin spectrum, a peak at 3394 cm^{-1} is observed, corresponding to the symmetrical stretching vibrations of the hydroxyl (–OH) group. The transmission bands obtained at 850 to 670 cm^{-1} are assigned to the C–H aromatic hydrocarbon bending vibration, while the bands at 1239 and 1652 cm^{-1} correspond to the C–O phenol stretching vibration and the C=O stretching vibration of aryl ketones, respectively.[35] The transmission band related to the symmetrical stretching vibrations of the (–OH) group is also found in the spectra of pristine TiO_2 and Au/TiO_2 nanoparticles, being more intense for the pristine and the non-centrifuged samples. In addition, a band at 1624 cm^{-1} can be identified as the bending mode of absorbed water molecules (Ti–OH). The band that extends from 860 to 500 cm^{-1} corresponds to the Ti–O–Ti bending mode. These results are consistent with the literature.[36]

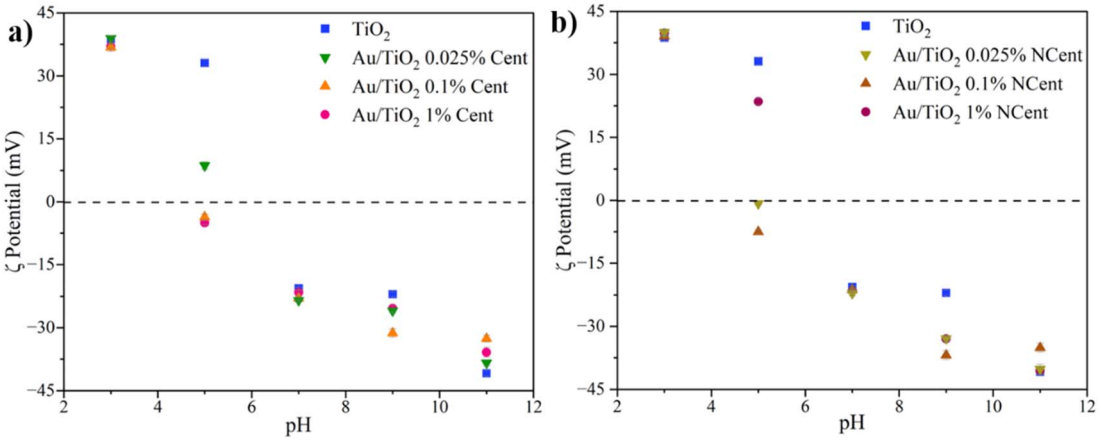

Fig. 6 Zeta potential of pristine TiO_2 and Au/TiO_2 nanoparticles, both (a) centrifuged and (b) non-centrifuged.

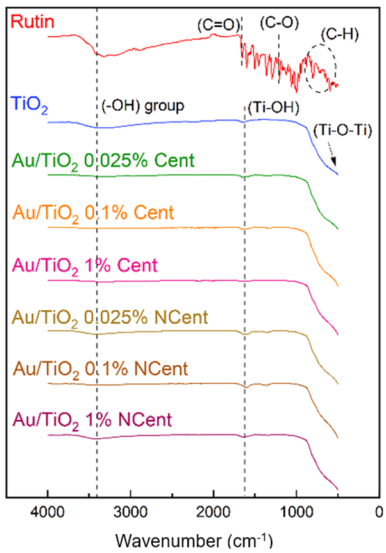

Fig. 7 ATR-FTIR spectra of rutin, pristine TiO_2 and synthesised Au/TiO_2, both (a) centrifuged and (b) non-centrifuged.

Finally, the nanoparticles' optical properties were studied through reflectance spectroscopy. The absorbance spectra for the pristine TiO_2 and the synthesised samples Au/TiO_2 0.025% Cent, Au/TiO_2 1% Cent, and Au/TiO_2 1% NCent are shown in Fig. 8. The expected UV light absorption peak observed in the literature for pristine TiO_2 at 300 nm was extended to 320 nm with the addition of Au nanoparticles.[37] Furthermore, a new absorption peak is identified in the visible region between 480 and 600 nm due to the SPR phenomenon related to the Au nanoparticles.[37] It is also observed that higher concentrations of Au nanoparticles and the lack of centrifugation steps lead to a more intense peak due to the samples' residual materials.

Table 2 summarises the band gap energies, E_g, of different samples obtained by applying the Tauc expression (eqn (2)).

The obtained band gap for pristine TiO_2 is 3.25 eV, consistent with the literature.[38–40] This value is reduced for the synthesised samples, with a lower limit of 2.52 to 2.68 eV, depending on Au concentration. This confirms that adding Au nanoparticles promotes absorption in the visible region (redshift) and influences absorption in the UV region.

Photocatalytic degradation of ciprofloxacin

The photocatalytic efficiency of the synthesised Au/TiO_2 nanoparticles is first tested through CIP (5 mg L^{-1}) degradation under UV radiation for 60 minutes. The photolysis effect on the degradation of CIP (5 mg L^{-1}) for UV and Xenon Lamp radiation is found in (ESI Fig. S13 and S14†) characteristic CIP absorption peak (277 nm) as a function of irradiation time. The obtained results reveal the negligible CIP degradation by photolysis both under UV and Xenon lamp radiation, which is related to the low absorbance displayed by CIP (absorbance peak 277 nm) in the wavelength range emission peak of both lamps (UV 365 nm and Xenon lamp >385 nm) – (ESI Fig. S15†). These first results are paramount to demonstrating CIP's photostability under UV and simulated sunlight radiation.

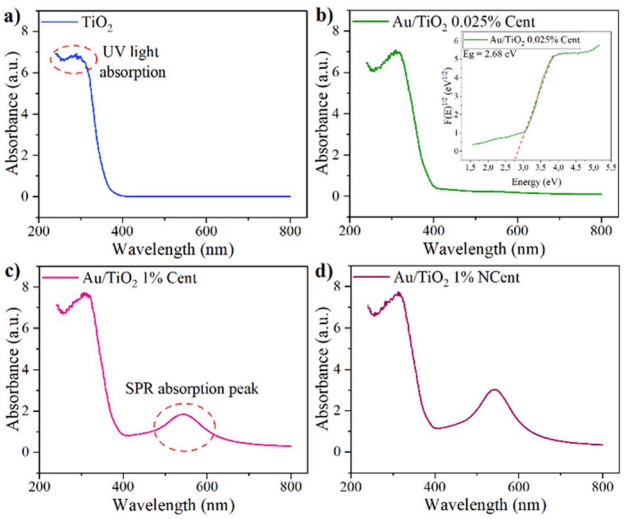

Fig. 8 Absorbance spectra of (a) pristine TiO_2 and synthesised (b) Au/TiO_2 0.025% Cent, (c) Au/TiO_2 1% Cent, (d) Au/TiO_2 1% NCent nanoparticles.

Table 2 Bandgap (E_g) energy values of pristine TiO_2 and synthesised Au/TiO_2 nanoparticles

	Sample	E_g (eV)	ΔE_g
	TiO_2	3.25	0.01
Cent	Au/TiO_2 0.025%	2.68	0.01
	Au/TiO_2 0.1%	2.62	0.01
	Au/TiO_2 1%	2.60	0.01
NCent	Au/TiO_2 0.025%	2.52	0.01
	Au/TiO_2 0.1%	2.59	0.01
	Au/TiO_2 1%	2.52	0.01

Table 3 Quantification of degraded CIP (5 mg L^{-1}) after photocatalysis under UV radiation and pseudo-first-order reaction rate constant, k, for pristine TiO_2 and synthesised Au/TiO_2 nanoparticles

	Sample	Adsorption (%)	Degradation (%)	k (min^{-1})	Δk
	TiO_2	2	66	0.023	0.005
Cent	Au/TiO_2 0.025%	1	75	0.026	0.002
	Au/TiO_2 0.1%	4	74	0.025	0.002
	Au/TiO_2 1%	6	74	0.024	0.002
NCent	Au/TiO_2 0.025%	32	65	0.020	0.001
	Au/TiO_2 0.1%	24	67	0.020	0.001
	Au/TiO_2 1%	22	58	0.016	0.002

The percentages of CIP adsorbed to the nanoparticles' surface and degraded through photocatalysis are calculated through the variation in CIP concentration between the control sample and the samples withdrawn at times $t = 0$ min and $t = 60$ min, respectively. From the graphs in Fig. 9, it is possible to draw the exponential line that best fits the data of each test and corresponds to the L–H equation (eqn (3)), from which the pseudo-first-order reaction rate constants k, are determined. The estimated values are summarised in Table 3.

The control sample of the original CIP solution is compared to those withdrawn after 30 minutes under agitation in the dark to quantify the adsorption phenomenon and establish the adsorption equilibrium. The results show that only 2% of CIP adsorbs on the surface of pristine TiO_2 nanoparticles. For the centrifuged samples, the adsorption percentage ranges from 1% to 6%, *i.e.*, it increases with the concentration of Au. This data is consistent with previous works indicating that Au also has an affinity with CIP molecules, favouring the adsorption process. A significant CIP adsorption increase is observed for the non-centrifuged samples, with percentages ranging from 22% to 32%. Demonstrating that, in the non-centrifuged samples, the presence of rutin is the predominant factor affecting the CIP adsorption, leading to stronger intermolecular forces and, consequently, higher adsorption percentages when compared to the centrifuged samples.[16,41,42]

The photocatalytic efficiency under UV radiation improves with the addition of Au. Pristine TiO_2 nanoparticles can degrade 66% of CIP. At the same time, all nanocomposites with Au concentrations of 0.025, 0.1, and 1 wt% that went through the centrifugation steps managed to degrade ~75% of CIP. With the functionalisation of pristine TiO_2, the recombination of electron–hole pairs is reduced since the excited electrons can be conducted to the Au nanoparticles.[16] This explains the improvement of photocatalytic efficiencies.

In contrast, the nanocomposites with Au concentrations of 0.025, 0.1, and 1 wt% that were not submitted to centrifugation degraded 65%, 67%, and 58% of CIP, respectively. The literature states that the functionalisation with high concentrations of noble metals leads to a shield effect that blocks the surface-active sites of TiO_2 nanoparticles. In this work, the variation of Au concentration does not seem to significantly affect the photocatalytic efficiency under UV radiation. In this work, rutin over the nanoparticle's surface leads to higher CIP adsorptions; it can be assumed that the adsorbed CIP reduces the radiation harvesting on the nanoparticles' surface.[16] This may explain the lower photocatalytic efficiencies regarding the centrifuged samples' efficiency.

Since rutin decreases photocatalytic efficiencies, only the centrifuged nanoparticles were considered for testing under simulated solar radiation for 180 minutes. Figure 10 presents the variation of CIP concentration as a function of irradiation time under simulated solar radiation.

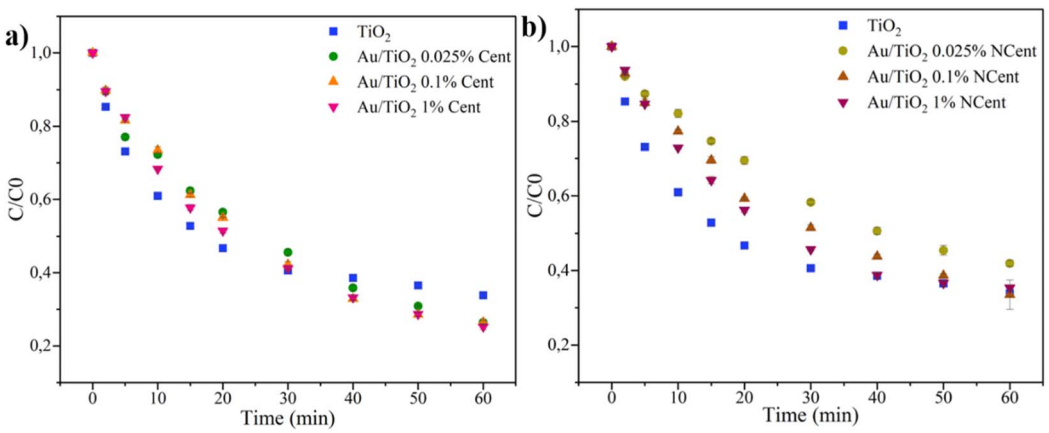

Fig. 9 Photocatalytic degradation of CIP (5 mg L^{-1}) under UV radiation for 60 minutes for pristine TiO_2 and synthesized Au/TiO_2 nanoparticles, both (a) centrifuged and (b) non-centrifuged.

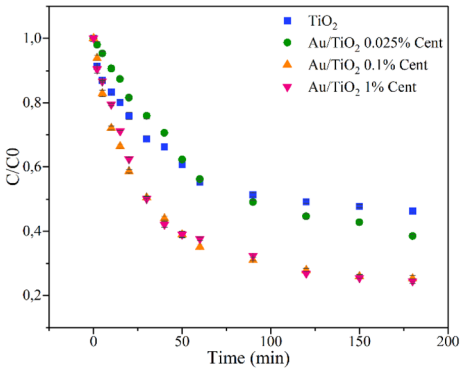

Fig. 10 Photocatalytic degradation of CIP (5 mg L^{-1}) under simulated solar radiation for 180 minutes for pristine TiO_2 and centrifuged Au/TiO_2 nanoparticles.

Table 4 Quantification of degraded CIP (5 mg L^{-1}) through photocatalysis under simulated solar radiation and pseudo-first-order reaction rate constant, k, for pristine TiO_2 and synthesised Au/TiO_2 nanoparticles

	Sample	Adsorption (%)	Degradation (%)	k (min^{-1}	Δk
	TiO_2	2	55	0.005	0.001
Cent	TiO_2Au 0.025%	8	62	0.006	0.001
	TiO_2Au 0.1%	4	75	0.010	0.002
	TiO_2Au 1%	7	75	0.010	0.002

Similarly to the photocatalytic tests under UV radiation, the percentages of adsorbed and degraded CIP and the pseudo-first-order reaction rate constants, k, are calculated through the L–H model and summarised in Table 4.

In this case, the adsorption percentages are similar to those in the degradation of CIP under UV radiation, while a more apparent difference in photocatalytic efficiencies is observed. The pristine TiO_2 nanoparticles can only degrade 55% of CIP, while the nanoparticles with Au concentrations of 0.025, 0.1, and 1 wt% succeeded in degrading 62%, 75%, and 75% of CIP, respectively. In the presence of gold, the excited electrons may be conducted to the gold particles, and the electron–hole recombination may be reduced, prolonging the generated holes' lifetime. Additionally, it leads to an absorption peak in the visible radiation region due to the SPR phenomenon.[16] These results also show that with higher Au concentrations, the photocatalytic efficiency increases, which is consistent with the intense absorption peaks in the visible region observed through reflectance spectroscopy (Fig. 8). However, it must be noted that higher concentrations of Au lead to a shielding effect that blocks the surface-active sites of TiO_2 nanoparticles. For example, when Au concentration is increased from 0.025 wt% to 0.1 wt%, the degradation efficiency is improved by 13%, and, in contrast, when the concentration is further increased to 1 wt%, the efficiency remains the same.

Considering this and from a sustainability standpoint, the samples with 0.1 wt% of Au nanoparticles present the most exciting results since they present the best photocatalytic efficiencies under UV and simulated solar radiation while utilising the least necessary resources. This is important to avoid waste and potential secondary contamination.[43] Thus, for this sample, Table 5 compares the photocatalytic efficiency obtained in the present work with two works that studied the effects of the functionalisation of TiO_2 nanoparticles with Au nanoparticles in the degradation of CIP under UV and simulated solar radiation. It must be noted that photocatalytic efficiency depends heavily on the specific experimental parameters of photocatalysis,[44] such as the radiation intensity, time of irradiation, and concentration of catalyst, Au, and contaminant.

In the case of degradation of CIP (5 mg L^{-1}) under UV radiation, Martins *et al.*[16] obtained the highest photocatalytic efficiency (91%). In contrast, Zheng *et al.*[45] achieved results similar to the present work (~77%). Since the UV lamps utilised were the same for every work, the efficiency difference is due to different photocatalyst concentrations. Regarding the degradation of CIP (5 mg L^{-1}) under similar simulated sunlight radiation (300 W m^{-2}), the previous works obtained a lower efficiency than the present work (~55%), even with a longer irradiation time, probably due to the lower Au concentration. The first work also obtained a lower efficiency of 49% due to an inferior radiation intensity (98 W m^{-2}). This comparative analysis shows that the TiO_2Au 0.1 wt% nanoparticles synthesised in this work display an improved performance under sunlight radiation range, making it a more cost-effective and sustainable approach. This feature is particularly relevant, as the intention is to offer an integral solution that contributes to sustainability during the production of the materials, based on avoiding the use of hazardous chemicals and, additionally, enabling the enhanced performance of the materials under free and clean sunlight radiation instead of costly UV radiation.[46]

Table 5 Comparison of the photocatalytic efficiency obtained in the present work with previous studies using TiO_2 nanoparticles for CIP degradation

Au concentration	Radiation	Time of irradiation (min)	Degradation (%)	Reference
0.1 wt%	UV	60	74	Present work
	Xenon lamp	180	75	
0.05 wt%	UV	30	91	16
	Xenon lamp	180	49	
	UV	60	77	45
	Xenon lamp	240	55	

Conclusions

The flavonoid rutin is utilised to functionalise pristine TiO_2 with Au nanoparticles. It is confirmed that using green synthesis methods does not alter the spheric morphology, size (~20 nm), and crystallinity of TiO_2 nanoparticles. A decrease in hydrodynamic size from 283 nm to ~150 nm with the addition of Au demonstrates the improvement of stability and prevention of aggregate formation. The band gap of the nanoparticles is improved from 3.14 eV to an average of 2.85 eV with the addition of Au, which allows the AU/TiO_2 nanocomposite to use sunlight radiation for the photocatalytic process efficiently.

The photocatalytic efficiency of pristine TiO_2 is 66% and 55% in the degradation of ciprofloxacin under UV radiation for 60 minutes and simulated solar radiation for 180 minutes, respectively. With the addition of Au nanoparticles onto the TiO_2 nanoparticles' surface and with centrifugation steps to remove rutin residue, these results are improved to an average of 74% and 71% under UV and visible radiation, respectively. With the photocatalytic tests under UV radiation, it was also shown that rutin on the nanoparticles reduces the photocatalytic efficiency to approximately 63%. The sample Au/TiO_2Au, 0.1% Cent, presents the best trade-off between the presence of Au and efficiency, as the sample containing 1% of Au does not show enhanced performance nor under UV or simulated sunlight radiation.

In conclusion, few works focus on developing green synthesis of photocatalysts, and fewer focus on the degradation of contaminants of emerging concern, such as pharmaceuticals. The herein-produced Au/TiO_2 nanocomposites using a natural rutin extract are confirmed as a promising approach for producing environmentally friendlier photocatalytic materials capable of efficiently removing contaminants of emerging concern under UV and simulated solar radiation. Further studies should be performed in the future with real water matrixes to confirm their potential and practicability in real scenarios.

Data availability

The data supporting this article have been included as part of the ESI.†

Conflicts of interest

There are no conflicts to declare.

Acknowledgements

The authors thank the Fundação para a Ciência e Tecnologia (FCT) for financial Support under the framework of Strategic Funding UIDB/04650/2020, UID/FIS/04650/2020 and UID/BIA/04050/2020 (DOI: 10.54499/UIDB/04050/2020). NGB was financed by the Ministry of Universities under application 33.50.460A.752 and by the European Union NextGenerationEU/PRTR through a contract Margarita Salas from the University of Vigo. P. M. M. thanks the FCT for the contract doi.org/10.54499/2020.02802.CEECIND/CP1600/CT0017. This study is part of the Advanced Materials programme and was supported by MCIN with funding from European Union NextGenerationEU (PRTR-C17.I1) as well as by IKUR Strategy under the collaboration agreement between Ikerbasque Foundation and Fundación BCMaterials on behalf of the Department of Education of the Basque Government.

References

1 H. Ritchie and M. Roser, *Clean Water and Sanitation*, https://ourworldindata.org/water-access, accessed 24 October 2022.
2 T. Deblonde, C. Cossu-Leguille and P. Hartemann, *Int. J. Hyg. Environ. Health*, 2011, **214**, 442–448.
3 *Ciprofloxacin*, https://www.nhs.uk/medicines/ciprofloxacin/, accessed 24 October 2022.
4 X. Wang, B. Li, T. Zhang and X. Li, *Desalination*, 2015, **370**, 7–16.
5 N. S. Shah, J. A. Khan, M. Sayed, Z. U. H. Khan, A. D. Rizwan, N. Muhammad, G. Boczkaj, B. Murtaza, M. Imran, H. M. Khan and G. Zaman, *Chem. Eng. J.*, 2018, **351**, 841–855.
6 A. R. Silva, *et al.*, *RSC Adv.*, 2016, **6**, 95494–95503.
7 C. Adams, Y. Wang, K. Loftin and M. Meyer, *J. Environ. Eng.*, 2002, **128**, 253–260.
8 R. V. Prihod'ko and N. M. Soboleva, *J. Chem.*, 2013, **2013**, 1–8.
9 M. F. Hanafi and N. Sapawe, *Mater. Today Proc.*, 2020, **31**, A158–A165.
10 G. Marcì and L. Palmisano, *Heterogeneous Photocatalysis*, Elsevier, 2019.
11 K. Kabra, R. Chaudhary and R. L. Sawhney, *Ind. Eng. Chem. Res.*, 2004, **43**, 7683–7696.
12 E. Baranowska-Wójcik, D. Szwajgier, P. Oleszczuk and A. Winiarska-Mieczan, *Biol. Trace Elem. Res.*, 2020, **193**, 118–129.
13 S. Hamad, C. R. A. Catlow, S. M. Woodley, S. Lago and J. A. Mejías, *J. Phys. Chem. B*, 2005, **109**, 15741–15748.
14 F. Parrino, F. R. Pomilla, G. Camera-Roda, V. Loddo and L. Palmisano, in *Titanium Dioxide (TiO_2) and Its Applications*, Elsevier, 2021, pp. 13–66.
15 X. Lin, H. Chen, Z. Hu, Y. Hou and W. Dai, *Solid State Sci.*, 2018, **83**, 181–187.
16 P. Martins, S. Kappert, H. Nga Le, V. Sebastian, K. Kühn, M. Alves, L. Pereira, G. Cuniberti, M. Melle-Franco and S. Lanceros-Méndez, *Catalysts*, 2020, **10**, 234.
17 S. Anu Mary Ealia and M. P. Saravanakumar, *IOP Conf. Ser. Mater. Sci. Eng.*, 2017, **263**, 1–15.
18 C. K. Venil, R. Usha and P. R. Devi, in *Nanomaterials*, Elsevier, 2021, pp. 283–298.
19 C. Hano and B. H. Abbasi, *Biomolecules*, 2021, **12**, 31.
20 N. Khan, S. Ali, S. Latif and A. Mehmood, *Nat. Sci.*, 2022, **14**, 226–234.
21 J. Rajkumari, C. M. Magdalane, B. Siddhardha, J. Madhavan, G. Ramalingam, N. A. Al-Dhabi, M. V. Arasu, A. K. M. Ghilan, V. Duraipandiayan and K. Kaviyarasu, *J. Photochem. Photobiol., B*, 2019, **201**, 111667.
22 K. Ashokkumar, K. Selvaraj and S. Devi, *J. Med. Plant Res.*, 2013, **7**(48), 3477–3483.

23 K. Patel and D. K. Patel, in *Bioactive Food as Dietary Interventions for Arthritis and Related Inflammatory Diseases*, Elsevier, 2019, pp. 457–479.
24 S. Dessai, M. Ayyanar, S. Amalraj, P. Khanal, S. Vijayakumar, N. Gurav, N. Rarokar, M. Kalaskar, S. Nadaf and S. Gurav, *Mater. Lett.*, 2022, **311**, 131639.
25 A. Monshi, M. R. Foroughi and M. R. Monshi, *World J. Nano Sci. Eng.*, 2012, **2**, 154–160.
26 J. Tauc, R. Grigorovici and A. Vancu, *Phys. Status Solidi B*, 1966, **15**, 627–637.
27 K. Vasanth Kumar, K. Porkodi and F. Rocha, *Catal. Commun.*, 2008, **9**, 82–84.
28 D. R. Eddy, M. D. Permana, L. K. Sakti, G. A. N. Sheha, S. Hidayat, T. Takei, N. Kumada and I. Rahayu, *Nanomaterials*, 2023, **13**, 704.
29 P. Martins, New generation of photocatalytic nanocomposites: production, characterization and environmental application, *PhD thesis*, Universidade do Minho, 2018.
30 P. M. Martins, V. Gomez, A. C. Lopes, C. J. Tavares, G. Botelho, S. Irusta and S. Lanceros-Mendez, *J. Phys. Chem. C*, 2014, **118**, 27944–27953.
31 A. P. Ramos, in *Nanocharacterization Techniques*, Elsevier, 2017, pp. 99–110.
32 P. M. Martins, B. Santos, H. Salazar, S. A. C. Carabineiro, G. Botelho, C. J. Tavares and S. Lanceros-Mendez, *Chemosphere*, 2022, **293**, 133548.
33 M. Song, L. Bian, T. Zhou and X. Zhao, *J. Rare Earth.*, 2008, **26**, 693–699.
34 R. G. Toro, M. Diab, T. de Caro, M. Al-Shemy, A. Adel and D. Caschera, *Materials*, 2020, **13**, 1326.
35 M. A. Saleemi, B. Alallam, Y. K. Yong and V. Lim, *Antioxidants*, 2022, **11**, 1853.
36 L. S. Chougala, M. S. Yatnatti, R. K. Linganagoudar, R. R. amble and J. S. Kadadevarmath, *J. Nano- Electron. Phys.*, 2017, **9**, 04005.
37 B. Tahir, M. Tahir and N. A. S. Amin, *Clean Technol. Environ. Policy*, 2016, **18**, 2147–2160.
38 C. Thambiliyagodage, *Environ. Nanotechnol. Monit. Manag.*, 2022, **18**, 100737.
39 X. Wang, L. Zhang, Y. Bu and W. Sun, *Appl. Surf. Sci.*, 2021, **540**, 148357.
40 K. Hofstadler, R. Bauer, S. Novalic and G. Heisler, *Environ. Sci. Technol.*, 1994, **28**, 670–674.
41 N. Ganbaatar, K. Imai, T. Yano and M. Hara, *Nano Converg.*, 2017, **4**, 38.
42 S. Shakiba, A. Hakimian, L. R. Barco and S. M. Louie, *Environ. Sci. Technol.*, 2018, **52**, 14158–14168.
43 I. Vasilachi, D. Asiminicesei, D. Fertu and M. Gavrilescu, *Water*, 2021, **13**, 181.
44 F. Zheng, P. M. Martins, J. M. Queirós, C. J. Tavares, J. L. Vilas-Vilela, S. Lanceros-Méndez and J. Reguera, *Chemosphere*, 2023, **313**, 137630.
45 F. Zheng, J. M. Queirós, P. M. Martins, R. F. de Luis, A. Fidalgo-Marijuan, J. L. Vilas-Vilela, S. Lanceros-Méndez and J. Reguera, *Colloids Surf. A Physicochem. Eng. Asp.*, 2023, **671**, 131594.
46 S. G. Kumar and L. G. Devi, *J. Phys. Chem. A*, 2011, **115**(46), 13211–13241.